Available online at www.sciencedirect.com
ScienceDirect
Journal of Power Sources 173 (2007) 240–248
JOURNAL OF POWER SOURCES
www.elsevier.com/locate/jpowsour

Simplified model for the direct methanol fuel cell anode☆

M.R. Shivhare, C.L. Jackson, K. Scott*, E.B. Martin

School of Chemical Engineering and Advanced Materials, Merz Court, Newcastle University, Newcastle upon Tyne, NE1 7RU, United Kingdom

Received 23 November 2006; received in revised form 28 April 2007; accepted 1 May 2007
Available online 7 May 2007

Abstract

A kinetic model for the anode of the direct methanol fuel cell (DMFC) is presented. The model is based on the generally accepted dual site mechanism of methanol oxidation, in aqueous solution, on well characterized Pt–Ru catalyst and it can predict the performance of the electrode as a function of cell temperature, anode potential and methanol concentration. In addition the model also generates data regarding the surface coverage of significant adsorbates involved in methanol oxidation on the dual site catalyst.

The analysis of the initial complex model confirms that a simplification in anode modelling can be made and some of the kinetic parameter can be reliably neglected. Based on this approach a fast and simplified three parameter model is derived from the same complex kinetic mechanism. The kinetic parameters of both models are estimated from experimental anode polarisation data from a 9 cm^2 DMFC operating with various methanol feed concentrations and temperatures. The models were developed in Lab VIEW and this has greatly simplified the simulation process, giving a model with ca. 85–95% fit on the experimental data. Depending on the computational speed available, and the desired complexity of problem at hand, either of the models can be used to give accurate model simulations for methanol fuel cell polarisations.

Keywords: Direct methanol fuel cell; Methanol oxidation kinetics; Surface coverage; Lab VIEW

1. Introduction

Low temperature liquid feed direct methanol fuel cells (DMFCs) are promising power sources for portable, stationary and vehicular applications given the relatively compact system design and higher energy densities when compared to existing technologies [1–3]. However, obstacles, such as the relatively poor kinetics of methanol oxidation at the anode, crossover of methanol through the membrane and the subsequent mixed potential at the cathode still hinder their widespread commercialisation [1–5].

The kinetics of the methanol oxidation reaction are determined by a complex mechanism involving adsorption of methanol on catalyst site followed by parallel and/or series reactions for electrochemical oxidation of methanol to CO_2. Based on the pioneering work of Bagotzky et al. [6] several mechanisms have been proposed in the literature to describe the methanol oxidation process [3,7–13]. Modern in situ spectroscopy methods like FTIRS and mass spectrometry have shed more light on the surface intermediates formed during the reaction and have been employed to elaborate upon the mechanism under different operating conditions. The Pt–Ru alloy is considered to be the present state-of-the-art candidate for practical anode catalysis in the DMFC and the common consensus is that the electro-oxidation of methanol on Pt–Ru occurs via a dual site mechanism [1–3,9–11,14–20,22].

To understand the complex kinetics in this work a semi empirical model based up on a dual site kinetic mechanism is presented. The model highlights the limiting reaction based on the kinetic parameters and elucidates the surface coverage of intermediate species formed in the reaction. The kinetic parameters deduced from the initial intricate mechanism are presented and further interpretation of these kinetic parameters has led to the formation of a simple kinetic expression which can be solved rapidly and used in real time DMFC simulations.

2. Experimental

In situ anode polarisation data was collected using an a single cell graphite (Ralph Coiden) fuel cell assembly etched with seven parallel channels of length 30 mm × 1 mm × 2 mm

☆ This paper was presented at the 2006 Fuel Cell Seminar in Honolulu, Hawaii.
* Corresponding author. Tel.: +44 191 222 8771; fax: +44 191 222 5292.
E-mail address: k.scott@ncl.ac.uk (K. Scott).

0378-7753/$ – see front matter © 2007 Elsevier B.V. All rights reserved.
doi:10.1016/j.jpowsour.2007.05.004

Nomenclature

a	activity
a/o	atomic ratio
C	concentration (mol m^{-3})
E	potential (V)
E_a	activation energy (kJ mol^{-1})
F	Faraday's constant (96487 A s mol^{-1})
j	current density (A m^{-2})
k_i	reaction rate constant for kinetic Eq. (1)
k'_i	reversible rate constant for kinetic Eq. (1)
n	number of electrons transferred
r	rate of reaction
R	gas constant (8.314 J mol^{-1} K^{-1})
T	temperature (K)

Greek letters

Γ	site density (mol m^{-2})
α_i	electrochemical transfer coefficient for kinetic Eq. (1)
β_i	transfer coefficient for kinetic Eq. (1)
θ_i	surface coverage for intermediate i

Subscripts

ads	adsorbed
CO, Pt	carbon monoxide on platinum sites
OH, Pt	hydroxyl ion on platinum site
OH, Ru	hydroxyl ion on ruthenium site
H_2O	water
M	methanol

creating an active surface area of 9 cm^2. An in-house manufactured membrane electrode assembly (MEA) was employed to generate the necessary data [15,16]. The MEA was fabricated using 1 mg$_{Pt}$ cm^{-2} at the anode and cathode with Pt–Ru/C 60wt.% a/o 1:1 and Pt/C 60wt.% from Etek, respectively. Catalyst layers contained 20wt.% Nafion® ionomer and catalyst layers were applied upon a micro-porous layer of 0.5 mgKB cm^{-2} (Ketjen Black) with a 20wt.% PTFE binder content deposited upon a TGP 090 20% WP (Toray) gas diffusion layer. The Electrodes were hot pressed to a Nafion® 117 membrane at 140 °C under a load of 50 kg cm^{-2} for 10 min and allowed to cool under pressure. The MEA was mounted inside the test cell and compressed to a torque of ca. 2 Nm. Conditioning over 24 h with intermittent polarisation resulted in reproducible performance.

Anode data was collected by using the cathode as a pseudo-reference electrode, by feeding a 5%.vol. hydrogen in nitrogen stream and polarising the cell between OCP and 700 mV [16] using liquid methanol as fuel at the anode side. Data were collected potentiostatically and at a potentiodynamic sweep rate of 2 mV s^{-2}, with minimal difference observed. Conditions of temperature and concentration were varied between 30–90 °C and 0.25–4 mol dm^{-3}, respectively, and the system were given ca. 2 h to equilibrate before testing.

3. Model development

3.1. Reaction mechanism

It is widely accepted that during methanol oxidation, the most significant reactions are the adsorption of methanol on the catalyst site and the oxidation of CO. Hence, in this work, a simplified and general reaction mechanism derived from a more complex mechanism was selected [8,9,18]. The simplified mechanism using dual site approach comprises the following steps:

3.1.1. On Pt sites

$$CH_3OH \underset{k'_1}{\overset{k_1}{\longleftrightarrow}} CH_3OH_{ads} \quad (1)$$

$$CH_3OH_{ads} \underset{k'_2}{\overset{k_2}{\longleftrightarrow}} CO_{ads,Pt} + 4H^+ + 4e^- \quad (2)$$

$$H_2O \underset{k'_{3,Pt}}{\overset{k_{3,Pt}}{\longleftrightarrow}} OH_{ads,Pt} + H^+ + e^- \quad (3a)$$

3.1.2. On Ru sites

$$H_2O \underset{k'_{3,Ru}}{\overset{k_{3,Ru}}{\longleftrightarrow}} OH_{ads,Ru} + H^+ + e^- \quad (3b)$$

3.1.3. Surface reaction

$$CO_{ads,Pt} + (OH_{ads,Pt} + OH_{ads,Ru}) \underset{k_4}{\overset{k_4}{\longrightarrow}} CO_2 + H^+ + e^- \quad (4)$$

It is assumed that reaction (3b) principally occurs on ruthenium (Ru) and reaction (1) occurs principally on platinum (Pt), as it is known that Ru is a poor electrocatalyst for methanol oxidation. Generally it is thought that the rate controlling step is reaction step (4) between the adsorbed species $CO_{ads,Pt}$ and OH_{ads}, which in turn depends on reaction steps (1–3) for the formation of adsorbed species. Thus, on the basis of this the rate of reaction can be written as:

$$r_4 = k_4\theta_{OH,Pt}\theta_{CO,Pt}\, e^{(((1-\beta_4)FE)/RT)} + k_4\theta_{OH,Ru}\theta_{CO,Pt}\, e^{(((1-\beta_4)FE)/RT)} \quad (5)$$

3.2. Assumptions

The assumptions used in the model are

i. The electrodes are at steady state.
ii. Isothermal and isobaric operation and the concentration gradient between the reacting site and the bulk fuel is negligible.
iii. Butler–Volmer kinetics is valid for the charge transfer steps.
iv. Only liquid phase is considered and CO_2 is assumed to be dissolved in the solution.
v. Methanol oxidation described by the kinetic expression Eqs. (1)–(4) follows the dual site mechanism thus surface coverage are independent of the adsorption rate of other species.

3.3. Analytical solution

The rates of changes of surface coverage of different species (θ_i) with respect to time are:

$$\Gamma\frac{d\theta_M}{dt} = k_1 C_M(1-\theta_{OH,Pt}-\theta_{CO,Pt}-\theta_{M,Pt}) - k_1'\theta_{M,Pt} + k_2'\theta_{CO,Pt}\, e^{(((1-\beta_2)FE)/RT)} - k_2\theta_{M,Pt}\, e^{((\alpha_2 FE)/RT)} \quad (6)$$

$$\Gamma\frac{d\theta_{CO,Pt}}{dt} = k_2\theta_M\, e^{((\alpha_2 FE)/RT)} - k_2'\theta_{CO,Pt}\, e^{(((1-\beta_2)FE)/RT)} - k_4\theta_{OH,Pt}\theta_{CO,Pt}\, e^{(((1-\beta_4)FE)/RT)} - k_4\theta_{OH,Ru}\theta_{CO,Pt}\, e^{(((1-\beta_4)FE)/RT)} \quad (7)$$

$$\Gamma\frac{d\theta_{OH,Pt}}{dt} = k_{3,Pt}a_{H_2O}(1-\theta_{OH,Pt}-\theta_{CO,Pt}-\theta_{M,Pt})e^{(((1-\beta_3)FE)/RT)} - k_{3,Pt}'\theta_{OH,Pt}\, e^{(((-\beta_3)FE)/RT)} - k_4\theta_{OH,Pt}\theta_{CO,Pt}\, e^{(((1-\beta_4)FE)/RT)} \quad (8)$$

$$\Gamma\frac{d\theta_{OH,Ru}}{dt} = k_{3,Ru}a_{H_2O}(1-\theta_{OH,Ru})e^{(((1-\beta_3)FE)/RT)} - k_{3,Ru}'\theta_{OH,Ru}\, e^{(((-\beta_3)FE)/RT)} - k_4\theta_{OH,Ru}\theta_{CO,Pt}\, e^{(((1-\beta_4)FE)/RT)} \quad (9)$$

Eq. (3a), the dissociation of water and adsorption of hydroxyl species upon platinum is known to be limited to relatively high potentials. Cyclic voltammetry and cell anode polarisation data have confirmed that OH-groups are preferentially formed on ruthenium at fairly low potentials (ca. 0.3 V versus dynamic hydrogen reference electrode (DHE)), whereas much higher potentials (ca. 0.9 V versus DHE) are required up on platinum [2,3,10,14,19,20]. On this basis, it can be assumed that adsorption of hydroxyl ions on Pt sites is negligible ($\theta_{OH,Pt} \approx 0$) and can be neglected from all the above equations. Thus, Eq. (5) is simplified to:

$$r_4 = k_4\theta_{OH,Ru}\theta_{CO,Pt}\, e^{(((1-\beta_4)FE)/RT)} \quad (10)$$

The case when adsorption of hydroxyl species also occurs on Pt, reaction (3a), is considered in the Appendix A along with the solution. This modelling procedure will contain additional three kinetic parameters hence it will be more time consuming and complex compared to the detailed model in manuscript.

At steady state surface coverage does not vary with time and the derivative becomes zero. Thus, with $a_{H_2O} = 1$, and $\theta_{OH,Pt} \approx 0$, the steady state solution of Eqs. (6)–(9) gives:

$$\theta_{CO,Pt} = \frac{k_1 C_M - \theta_M(k_1 C_M + k_2\, e^{((\alpha_2 FE)/RT)} + k_1')}{k_1 C_M - k_2'\, e^{(((1-\beta_2)FE)/RT)}} \quad (11)$$

$$\theta_{CO,Pt} = \frac{k_2\theta_M\, e^{((\alpha_2 FE)/RT)}}{k_2'\, e^{(((1-\beta_2)FE)/RT)} + k_4\theta_{OH,Ru}\, e^{(((1-\beta_4)FE)/RT)}} \quad (12)$$

$$\theta_{CO,Pt} = \frac{k_{3,Ru}\, e^{(((1-\beta_3)FE)/RT)} - k_{3,Ru}\theta_{OH,Ru}\, e^{(((1-\beta_3)FE)/RT)} - k_{3,Ru}'\theta_{OH,Ru}\, e^{(((-\beta_3)FE)/RT)}}{k_4\theta_{OH,Ru}\, e^{(((1-\beta_4)FE)/RT)}} \quad (13)$$

The above simultaneous equations can be solved to give the surface coverage of $\theta_{OH,Ru}$ and $\theta_{CO,Pt}$, and thus to find the overall rate of reaction (r_4). This can then be combined with Faradays law to give:

$$\therefore\ j = nFk_4\theta_{OH,Ru}\theta_{CO,Pt}\, e^{(((1-\beta_4)FE)/RT)} \quad (14)$$

The complexity in the solution of this problem arises as the quadratic must be solved at multiple potentials, at various temperatures and concentrations adjusting seven rate constants, which presents a vast number of permutations. The model was therefore constructed using Lab VIEW software from National Instruments [21]. An alternative approach in which adsorption of OH on Pt is also considered, is given in the Appendix A. It should be noted that addition of more reaction steps increases the number of parameters to be analysed and adds complexity in solving the non-linear equation [12,13,17]. The basis of semi empirical modelling is generally based on principal of parsimony and fast computational speed. A detailed model, as shown in the Appendix A, is complex and slow to compute. However, detailed models when supplement with transient electrochemical measurements from modern tools can lead to the extraction of accurate kinetic parameters and limiting steps [3,20]. An additional factor in the model used here is that the methanol oxidation is considered as a single four electron step. Introduction of single electron transfers involving more intermediates adds to the complexity and creates a large number of parameters which generally would not be amenable to estimation using the experimental data available.

4. Results and discussion

4.1. Model validation

To date the trend in validation has been quite varied. Several authors verify their models using cell polarisation data alone without a reference electrode [1,2] whereas others have verified their anode models against anode polarisation data using a hydrogen evolving cathode [4,5]. However, polarisation data alone, without any consideration of whether the model fits the Tafel slope for the data or whether the model can predict the activation energy within a realistic range has rarely been reported. The model was deemed to provide a suitably accurate fit when the R^2 statistics for the actual and calculated curves was greater than 90%. These additional considerations, linked with the fact that coverage of the catalyst is restricted to values between 0 and 1, all enable tighter determination of the derived kinetic constants with varying temperature and concentration. In order to achieve such a complex validation technique, additional programming was performed in Lab VIEW. Fig. 1 shows the fit of model to the experimental data from a cell operating at 30, 60 and 90 °C respectively with varying methanol concentrations of 0.25, 0.5, 1, 2 and 4 M.

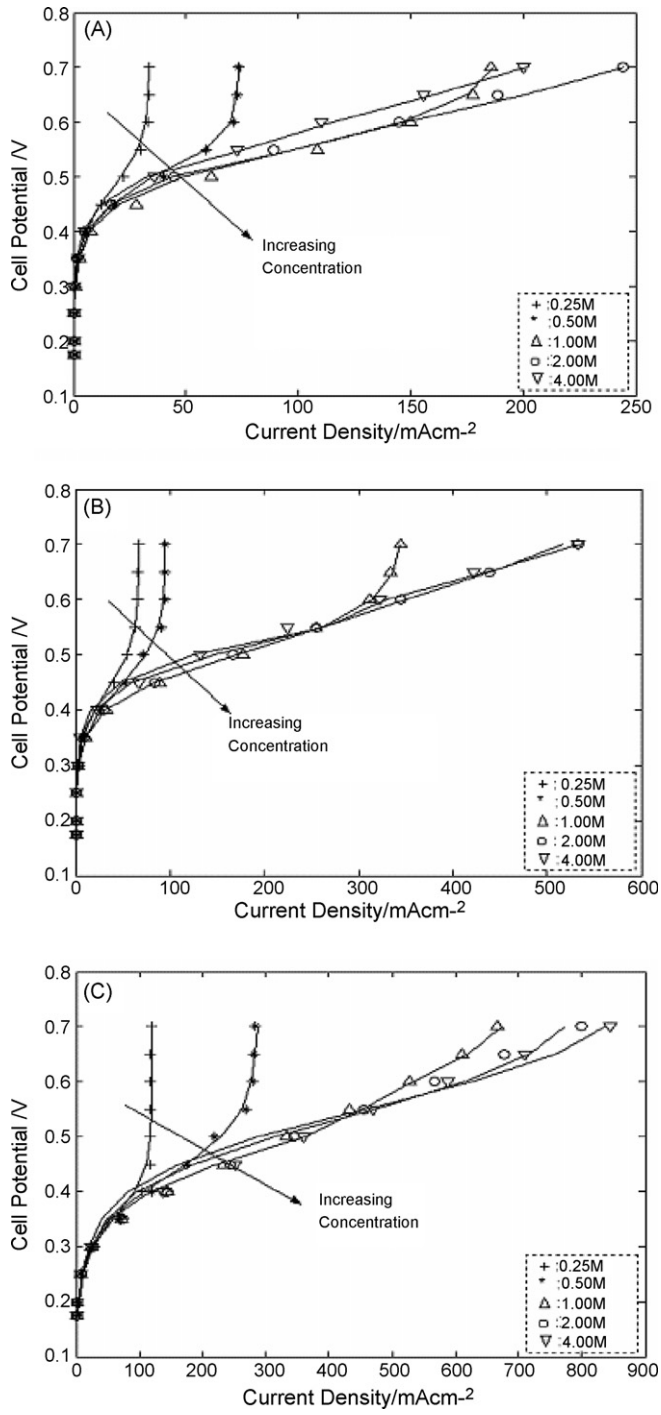

Fig. 1. Model (line) vs. experimental fit for cell at (A) 30 °C, (B) 60 °C and (C) 90 °C with varying methanol concentrations.

The onset potential of the methanol oxidation reaction occurred at ca. 0.250 V versus DHE. From Fig. 1 it can bee seen that the kinetic region is not a function of concentration whilst an increase in concentration led to increasingly large limiting currents that above 2 M were outside the range of the experimental data, due to the potential limitation of ruthenium dissolution above 0.750 V. The model is based on kinetics and it is essential that it fits the experimental data at the low current end of the polarisation. Hence, along with the anode polarisation curve

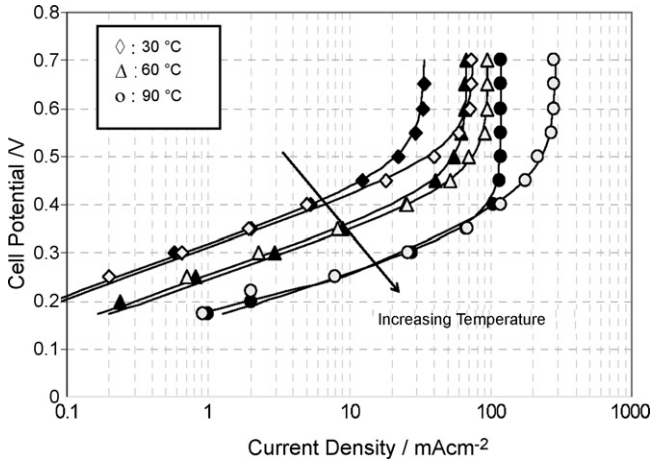

Fig. 2. Model (line) vs. experimental fit on a Tafel plot at 0.25 M (black marker) and 0.5 M (white marker) at varying temperature of 30, 60 and 90 °C.

in this work the model was also fitted on a Tafel plot. Fig. 2 shows the fit of the polarisation data of Fig. 1 for 0.25 M and 0.5 M at varying cell temperature on a Tafel plot which magnifies the low current dependence upon potential. The model predicted the Tafel slope for the reaction accurately, confirming its reliable prediction of the kinetic behaviour. Since experimental factors such a membrane electrode manufacturing technique and cell test design can affect the mass transport region significantly, in this work more attention was given on fitting the data at low end of polarisation rather than the mass transport region, which will be considered in future publications.

A further confirmation that the model is functioning correctly was the correlation of the kinetic currents of the predicted Tafel slope at one potential and three temperatures. The activation energy was derived from the Arrhenius relationship and used to gauge whether or not the solution was within a suitable range between 30 and 70 kJ mol^{-1} [11,22]. Fig. 3 shows the Arrhenius plot along with slope for the data generated from Fig. 2. The activation energy generated from model was between 42 and 45 kJ mol^{-1}. Table 1 shows the constants and kinetic parameters used in the model.

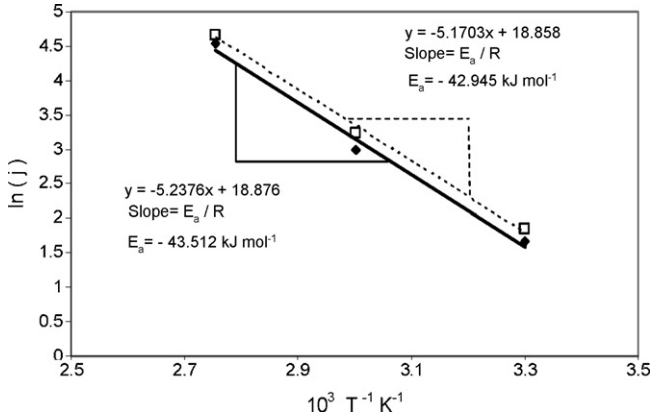

Fig. 3. Arrhenius plot from the model vs. experimental fit for cell at 0.25 M (black marker) and 0.5 M (white marker).

Table 1
Constants and parameters used in the detail kinetic model

Parameters	Fit at 30 °C	Fit at 60 °C	Fit at 90 °C
k_1	2.6×10^{-6} (m s^{-1})	3.3×10^{-6} (m s^{-1})	9.95×10^{-6} (m s^{-1})
k'_1	1×10^{-11} (mol m^{-2} s)	1×10^{-11} (mol m^{-2} s)	1×10^{-11} (mol m^{-2} s)
k_2	1.91×10^{-8} (mol m^{-2} s)	7×10^{-8} (mol m^{-2} s)	1.35×10^{-6} (mol m^{-2} s)
k'_2	1×10^{-13} (mol m^{-2} s)	1×10^{-13} (mol m^{-2} s)	1×10^{-13} (mol m^{-2} s)
$k_{3,Ru}$	6.12×10^{-8} (mol m^{-2} s)	5.3×10^{-7} (mol m^{-2} s)	4.8×10^{-6} (mol m^{-2} s)
$k'_{3,Ru}$	3.63×10^{-1} (mol m^{-2} s)	9×10^{-1} (mol m^{-2} s)	9×10^{-1} (mol m^{-2} s)
k_4	3.91×10^{-2} (mol m^{-2} s)	7.62×10^{-2} (mol m^{-2} s)	9.85×10^{-2} (mol m^{-2} s)
α_2	0.57	0.65	0.80
β_2	0.5	0.5	0.5
β_3	0.5	0.5	0.5
β_4	0.5	0.5	0.5

4.2. Surface coverage

The advantage of using such a detail kinetic model lies in the determination of surface coverage of intermediate species on the catalyst site. Fig. 4 depicts the surface coverage of methanol ($\theta_{M,Pt}$) and hydroxyl ion ($\theta_{OH,Ru}$) on Pt–Ru catalyst sites at different temperature. From these figures, it can be seen that the surface coverage of methanol decreases with the increase in cell potential whereas the surface coverage of hydroxyl ion increases with the increase in cell potential. It can also be seen that the temperature and concentration have opposite effects on hydroxyl and methanol coverage on the catalyst site. An increase in temperature causes $\theta_{M,Pt}$ to decrease and $\theta_{OH,Ru}$ to increase whereas an increase in methanol feed concentration causes an increase in $\theta_{M,Pt}$ and decrease in $\theta_{OH,Ru}$. Overall, on the basis of the response of the surface coverage's of intermediate species to change in temperature and concentration, it can be concluded that the anode polarisation curve shows a strong dependence on these two operating parameters [5,12,13,17–19,22,23]. From Figs. 1 and 4 it can be observed that the limiting current of the anode polarisation curve is reached when either the surface coverage of methanol approaches zero or when the surface coverage of hydroxyl group approaches a saturation limit. This limiting current can be clearly observed in case of 0.25 and 0.5 M methanol concentration. The kinetic model also depicted the surface coverage of CO on the catalyst site, but over the entire potential range $\theta_{CO,Pt}$ was close to zero. This is reasonable as the 1:1 a/o of the Pt:Ru catalyst is commonly employed to ensure that there is a high $\theta_{OH,Ru}$ presence to react with adsorbed CO at source rather than requiring it to diffuse across the crystal surface and poison the catalyst, as it does on pure platinum. These results are in agreement with other literature [11–14,22,24].

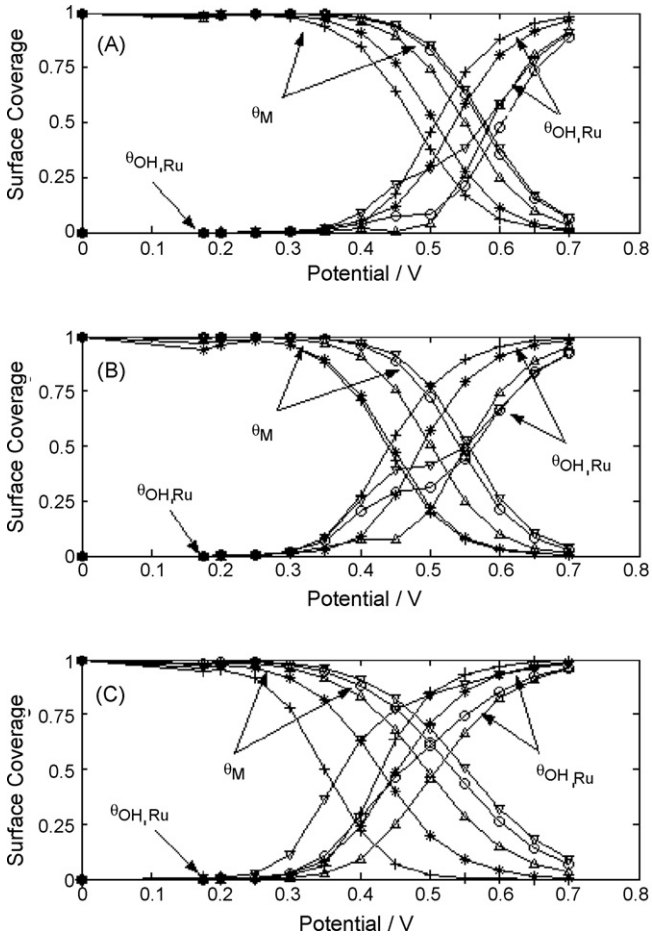

Fig. 4. Surface coverage of intermediate species on Pt–Ru catalyst sites predicted by the model with varying methanol concentrations (+: 0.25 M, *: 0.5 M, △: 1 M, ◯: 2 M, ∇: 4 M) at (A) 30 °C, (B) 60 °C and (C) 90 °C, respectively.

4.3. Limiting reaction

It was observed that the variation in the kinetic parameters presented in Table 1 had a significant effect upon the shape and fit of the modelled curve. Variation of all of the rate constants resulted in an onset potential of ca. 0.250 V versus DHE or above in all cases which is in good agreement with the experimental data. Fig. 5 shows the effect of varying the most significant factors α_2, k_1 and k_2 on the anode polarisation curve. Variation in k_1 was found only to affect the limiting current of the curve as shown in Fig. 5B. Variation in α_2 and k_2 had a significant effect upon the onset potential and the Tafel slope of the reaction as shown in Fig. 5A and C, respectively. The kinetic parameters of the reverse reactions, particularly k'_1 and k'_2, did not affect the polarisation curve or surface coverage of intermediates, although $k'_{3,Ru}$ had a minor effect on the polarisation curve and surface coverage of intermediates. Rate constants $k_{3,Ru}$ and

k_4 were found to have a less significant effect upon the curve in the fitting range, indicating that, for this model, methanol adsorption and oxidation to CO was the rate limiting process and that sufficient adsorbed hydroxyl species were available for a much faster complete oxidation of CO to CO_2. This was also demonstrated by low surface coverage of CO on the catalyst site.

5. Simplified model

The kinetic model described above fits the experimental data well but it is complex, taking a considerable amount of time to compute. Variations in the kinetic parameters presented in Table 1 depicted that some kinetic parameters have less effect or almost no effect on the polarisation curve. Particularly the reverse reaction constants k_1' and k_2', suggest that they can be assumed to be negligible in comparison to forward reaction constants. Exclusion of these constants resulted in a mechanism similar to that proposed by Gasteiger et al. [10,14], which simplified Eq. (6) further to:

$$\Gamma\frac{d\theta_M}{dt}=k_1C_M(1-\cancelto{0}{\theta_{OH,Pt}}-\theta_{CO,Pt}-\theta_M)-\cancelto{0}{k_1'\theta_M}+\cancelto{0}{k_2'\theta_{CO,Pt}}e^{\left(\frac{(1-\beta_2)FE}{RT}\right)}-k_2\theta_M e^{\left(\frac{\alpha_2 FE}{RT}\right)}$$

At steady state this gives

$$\therefore \theta_M = \frac{k_1C_M(1-\theta_{CO,Pt})}{k_2\,e^{((\alpha_2 FE)/RT)}+k_1C_M}$$

In the detail kinetic model it was seen that the surface coverage of CO was very low and is almost negligible above 0.3 V. On this basis, it was assumed that, $1-\theta_{CO}\approx 1$. Thus, the above equation further simplifies to:

$$\therefore \theta_M = \frac{k_1C_M}{k_2\,e^{((\alpha_2 FE)/RT)}+k_1C_M} \quad (15)$$

Similarly Eq. (7) further simplifies to:

$$\Gamma\frac{d\theta_{CO,Pt}}{dt} = k_2\theta_M\,e^{((\alpha_2 FE)/RT)} - k_4\theta_{OH,Ru}\theta_{CO,Pt}\,e^{(((1-\beta_4)FE)/RT)}$$

$$\therefore k_4\theta_{OH,Ru}\theta_{CO,Pt}\,e^{(((1-\beta_4)FE)/RT)} = k_2\theta_M\,e^{((\alpha_2 FE)/RT)} \quad (16)$$

Substituting Eq. (16) into Eq. (14) results in

$$\therefore j = nFk_2\theta_M\,e^{((\alpha_2 FE)/RT)}$$

Substituting, θ_M, from Eq. (15) in above equation and simplifying it:

$$\therefore j = nFk_2\,e^{((\alpha_2 FE)/RT)}\left(\frac{k_1C_M}{k_2\,e^{((\alpha_2 FE)/RT)}+k_1C_M}\right) \quad (17)$$

Fig. 6 demonstrates the fit of the above simplified model to the experimental data of cell at 30, 60 and 90 °C with varying methanol concentrations. From these figures it can be seen that the simplified model also fits the data well but with less accuracy, R^2 statistics 85–90%, as compared to the detailed kinetic model with R^2 statistics 90–95%.

The model was also fitted to the Tafel plot and the activation energy derived in this case were between 42 and 49 kJ mol^{-1}, which was slightly higher than the detailed model but still within the acceptable range [11,22]. The drawback of the simplified model was that it cannot depict the surface coverage of intermediates involved in the mechanism. The kinetic parameters derived from the simplified model are shown in Table 2.

A further rearrangement of constant k_1 in Eq. (17) gave:

$$\therefore j = \frac{nFk_2\,e^{((\alpha_2 FE)/RT)}C_M}{C_M+(k_2/k_1)e^{(((1-\alpha_2)FE)/RT)}} \quad (18)$$

The above Eq. (18) is similar to Meyers and Newman [25] but the constants have different interpretations and significance. Moreover, in this work the above simplified equation is derived step by step from the complex kinetic mechanism on the basis of proven assumptions.

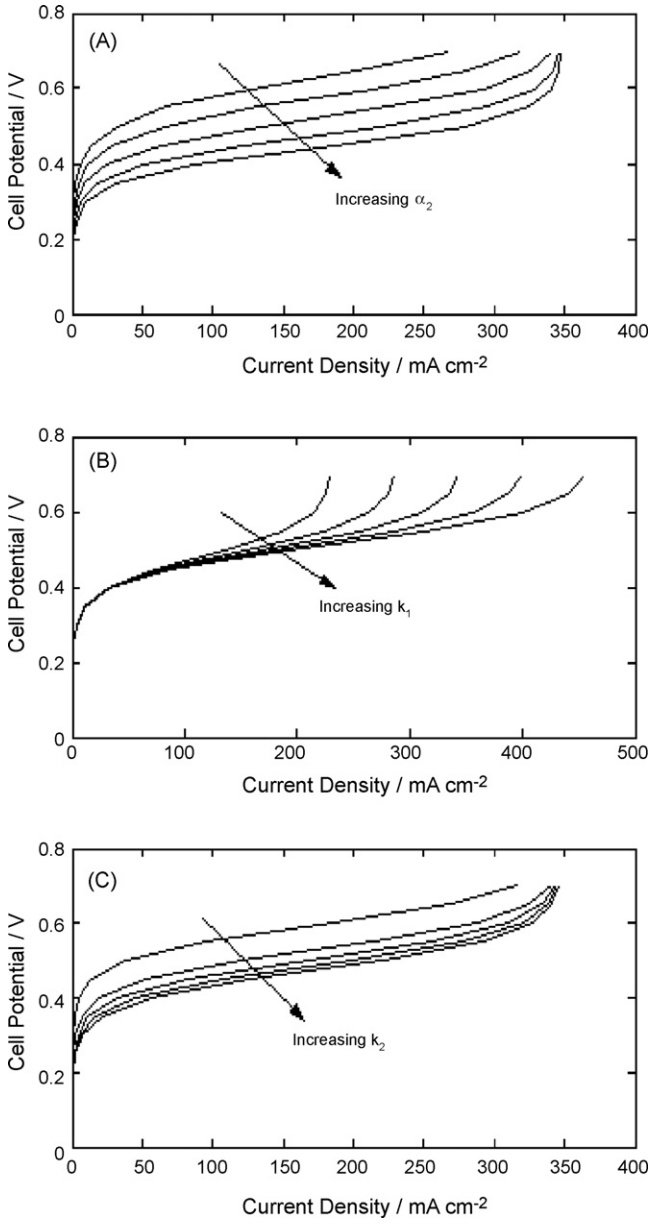

Fig. 5. Effect of varying the influential parameters (A) α_2, (B) k_1 and (C) k_2, respectively, on the anode polarisation curve.

Table 2
Constants and parameters used in the simplified model

Parameters	Fit at 30 °C	Fit at 60 °C	Fit at 90 °C
k_1	2.6×10^{-7} (m s^{-1})	3.3×10^{-7} (m s^{-1})	9.95×10^{-7} (m s^{-1})
k_2	1.3×10^{-9} (mol m^{-2} s)	5.04×10^{-9} (mol m^{-2} s)	1.53×10^{-7} (mol m^{-2} s)
α_2	0.60	0.67	0.80

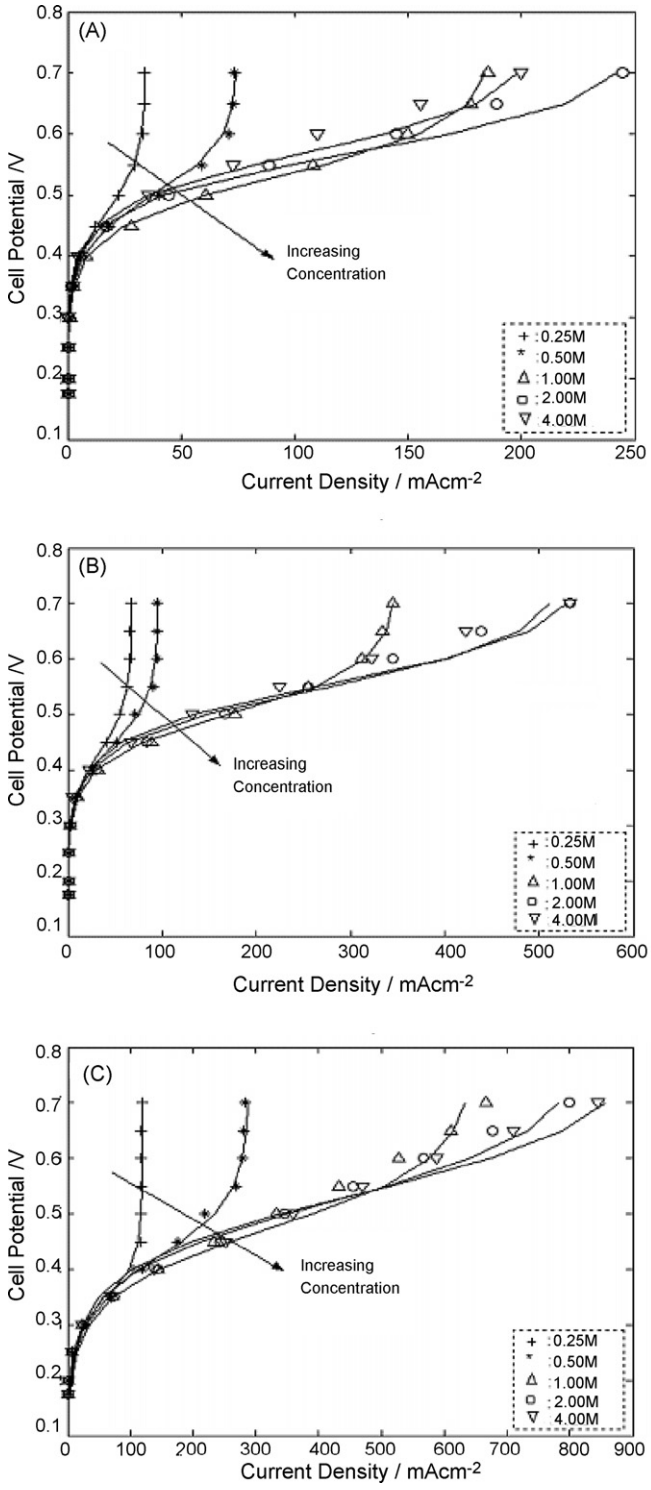

Fig. 6. Model (line) vs. experimental fit for cell at (A) 30 °C, (B) 60 °C and (C) 90 °C with varying methanol concentrations.

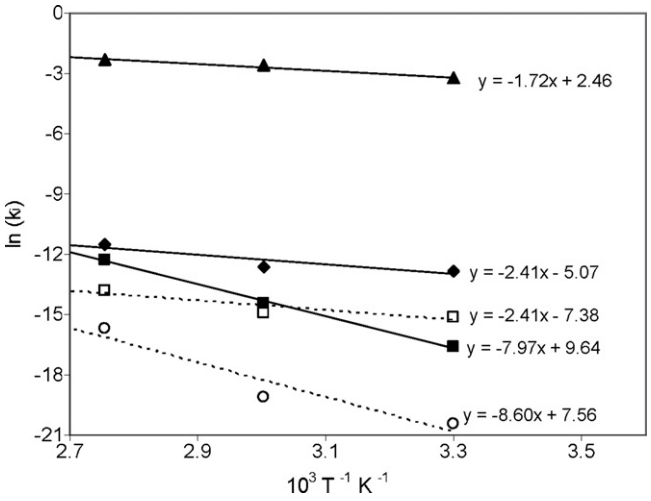

Fig. 7. Arrhenius plot of the kinetic parameters for comparison of resulting activation energy with other published results (♦: k_2, ■: $k_{3,Ru}$, ▲: k_4, □: k_1 (simplified model), ◯: k_2 (simplified model)).

Finally the parameters obtained by both the detailed model and simplified model were compared with other published results. The resulting kinetic parameters from both the modelling procedure were in accord with other literature [12,13,25,26]. Moreover, the activation energy obtained by plotting the Arrhenius plots, as shown in Fig. 7, also agreed with the published results [11,19,22]. Based on the previous work [17,18] and the models derived here it was found that the simplified model, given by Eqs. (17 and 18), involved the three significant kinetic parameters (α_2, k_1 and k_2) which were mainly responsible for describing the behaviour of anode polarisation curve as a function of cell temperature, anode potential and methanol concentration. The detailed models, given by Eq. (14) and Eq. (A.2), due to the presence of above significant parameters describe the polarisation behaviour and in addition, due to the presence of other kinetic parameters, it's useful in revealing the surface coverage intermediates on the catalyst site. The detailed models can give slightly more accurate results over the full range of anode potentials, although the simpler model is sufficient for most simulations.

6. Conclusion

A complex methanol oxidation mechanism was studied with the help of detail kinetic model. The surface coverage of intermediate species formed during the reaction were calculated and agreed with the results from other literature [12,13,19]. The model calculates anode polarisation behaviour on the basis of surface coverage and shows that the limiting current is reached

when the surface coverage of adsorbed methanol approaches zero or when the surface coverage of hydroxyl group approaches the saturation limit. The model highlights the subtle balance between the methanol adsorption and subsequent oxidisation to CO on the dual site catalyst and identifies them as the limiting steps rather than the surface oxidation of CO to CO_2. It was observed that by varying the kinetic rate constants a surface coverage of intermediates species can be manipulated while still obtaining a reasonable fit to the anode polarisation curve. To further validate the kinetic constants and the modelled coverage at particular operating conditions, the behaviour of intermediate species with respect to temperature, concentration and potential should be confirmed by the use of modern spectroscopy tools like the Fourier Transform Infra-red Spectroscopy (FTIRS) [3,20,24] and corroborated with the model.

Further refinement of this model can be achieved by adding more realistic conditions to the original reaction expressions. This could include non-ideality of the platinum and ruthenium distribution which would influence the impact of k_3 and k_4 and the addition of rate expressions for the more significant complex and stable intermediates. This aspect of modelling is the subject of ongoing work in the laboratories at Newcastle University.

The simplified model derived from the complex mechanism gives a faster approximation of anode performance. This would be useful if coupled with a diffusion model for the prediction of performance along a flow field channel or through the Nafion® membrane. Overall, depending on the computational speed and complexity of problem at hand, either of the models can be used for complete cell or stack studies using kinetic data.

Acknowledgements

M.R. Shivhare gratefully acknowledges the scholarship from Centre of Process Analytics and Control Technology (CPACT), Newcastle, UK. C.L. Jackson thanks the EPSRC for support during a PhD studentship. The work was performed in research facilities provided through an EPSRC/HEFCE Joint Infrastructure Fund Award no. JIF4NESCEQ.

Appendix A

In this modelling procedure the surface coverage of hydroxyl ion on Pt site is considered and it is assumed that the reaction of OH_{ads} with $CO_{ads,Pt}$ on both Pt and Ru sites occurs at different rates which adds another two kinetic parameter to the model. Thus, the rate of reaction is given by:

$$r_4 = k_{4,\mathrm{Pt}}\theta_{\mathrm{OH,Pt}}\theta_{\mathrm{CO}}\,\mathrm{e}^{(((1-\beta_4)\mathrm{FE})/RT)} + k_{4,\mathrm{Ru}}\theta_{\mathrm{OH,Ru}}\theta_{\mathrm{CO}}\,\mathrm{e}^{(((1-\beta_4)\mathrm{FE})/RT)} \quad (A.1)$$

$$\therefore\ j = nF(k_{4,\mathrm{Pt}}\theta_{\mathrm{OH,Pt}} + k_{4,\mathrm{Ru}}\theta_{\mathrm{OH,Ru}})\theta_{\mathrm{CO}}\,\mathrm{e}^{(((1-\beta_4)\mathrm{FE})/RT)} \quad (A.2)$$

By assuming the activity of water equal to unity the steady state solution in this case can be further simplified to:

$$\theta_{\mathrm{CO,Pt}} = \frac{k_1 C_{\mathrm{M}} - \theta_{\mathrm{M}}(k_1 C_{\mathrm{M}} + k_1' + k_2\,\mathrm{e}^{((\alpha_2\mathrm{FE})/RT)}) - k_1 C_{\mathrm{M}}\theta_{\mathrm{OH,Pt}}}{k_1 C_{\mathrm{M}} - k_2'\,\mathrm{e}^{(((1-\beta_2)\mathrm{FE})/RT)}} \quad (A.3)$$

$$\theta_{\mathrm{CO,Pt}} = \frac{k_2\theta_{\mathrm{M}}\,\mathrm{e}^{((\alpha_2\mathrm{FE})/RT)}}{k_2'\,\mathrm{e}^{(((1-\beta_2)\mathrm{FE})/RT)} + k_4\theta_{\mathrm{OH,Pt}}\,\mathrm{e}^{(((1-\beta_4)\mathrm{FE})/RT)} + k_4\theta_{\mathrm{OH,Ru}}\,\mathrm{e}^{(((1-\beta_4)\mathrm{FE})/RT)}} \quad (A.4)$$

$$\theta_{\mathrm{CO,Pt}} = \frac{k_{3,\mathrm{Pt}}(1-\theta_{\mathrm{OH,Pt}}-\theta_{\mathrm{M}})\mathrm{e}^{(((1-\beta_3)\mathrm{FE})/RT)} - k_{3,\mathrm{Pt}}'\theta_{\mathrm{OH,Pt}}\,\mathrm{e}^{(((-\beta_3)\mathrm{FE})/RT)}}{k_{3,\mathrm{Pt}}\,\mathrm{e}^{(((1-\beta_3)\mathrm{FE})/RT)} + k_{4,\mathrm{Pt}}\theta_{\mathrm{OH,Pt}}\,\mathrm{e}^{(((1-\beta_4)\mathrm{FE})/RT)}} \quad (A.5)$$

$$\theta_{\mathrm{CO,Pt}} = \frac{k_{3,\mathrm{Ru}}(1-\theta_{\mathrm{OH,Ru}})\mathrm{e}^{(((1-\beta_3)\mathrm{FE})/RT)} - k_{3,\mathrm{Ru}}'\theta_{\mathrm{OH,Ru}}\,\mathrm{e}^{(((-\beta_3)\mathrm{FE})/RT)}}{k_4\theta_{\mathrm{OH,Ru}}\,\mathrm{e}^{(((1-\beta_4)\mathrm{FE})/RT)}} \quad (A.6)$$

These non-linear equations can be solved further by using mathematical software like Maple and the solution can be incorporated into (A.1) and (A.2) to find the respective rate constant and subsequently the current density [17]. This modelling procedure will contain additional three kinetic parameters ($k_{3,\mathrm{Pt}}$, $k_{3,\mathrm{Pt}}'$, $k_{4,\mathrm{Pt}}$) hence it will be more time consuming and complex compared to the detail model in manuscript.

References

[1] R. Dillon, S. Srinivasan, A.S. Arico, V. Antonucci, J. Power Sources 127 (1/2) (2004) 112–126.
[2] T. Schultz, S. Zhou, K. Sundmacher, Chem. Eng. Technol. 24 (12) (2001) 1223–1233.
[3] S. Wasmus, A. Kuver, J. Electroanal. Chem. 461 (1999) 14–31.
[4] A. Heinzel, V.M. Barragan, J. Power Sources 84 (1) (1999) 70–74.
[5] J. Ge, H. Liu, J. Power Sources 142 (1/2) (2005) 56–69.
[6] V.S. Bagotzky, Y.B. Vassiliev, O.A. Khazova, J. Electroanal. Chem. 81 (2) (1977) 229–238.
[7] A. Hamnett, Catal. Today 38 (4) (1997) 445–457.
[8] T. Frelink, W. Visscher, J.A.R. Van Veen, Langmuir 12 (15) (1996) 3702–3708.
[9] T. Frelink, W. Visscher, J.A.R. Van Veen, Surf. Sci. 335 (1995) 353.
[10] H.A. Gasteiger, N. Markovic, P.N. Ross, E.J. Cairns, J. Phys. Chem. 97 (46) (1993) 12020.
[11] H.A. Gasteiger, N. Markovic, P.N. Ross, E.J. Cairus, J. Electrochem. Soc. 141 (7) (1994) 1795.
[12] J. Nordlund, G. Lindbergh, J. Electrochem. Soc. 149 (9) (2002) A1107–A1113.
[13] J. Nordlund, G. Lindbergh, J. Electrochem. Soc. 151 (9) (2004) A1357–A1362.
[14] N.M. Markovic, H.A. Gasteiger, P.N. Ross, X. Jiang, Surface Structure and Electrochemical Reactivity, vol. 40, Pergamon Press, 1995, p. 91.
[15] C. Jackson, G. Murgia, K. Scott, P. Argyropoulos, A. Shukla, Fuel Cell Seminar, Palm Springs, 2002, pp. 17–20.
[16] C. L. Jackson, Newcastle University, Newcastle upon Tyne, 2006, p. 269.
[17] M.R. Shivhare, R.G. Allen, K. Scott, A.J. Morris, E.B. Martin, J. Electroanal. Chem. 595 (2006) 145–151.
[18] K. Scott, P. Argyropoulos, J. Power Sources 137 (2) (2004) 228–238.
[19] P.S. Kauranen, E. Skou, J. Munk, J. Electroanal. Chem. 404 (1) (1996) 1–13.
[20] U. Krewer, M. Christov, T. Vidakovic, K. Sundmacher, J. Electroanal. Chem. 589 (2006) 148–159.

[21] National Instruments Corporation, Lab VIEW course manual, Basics I and II, March 2004.
[22] S.L. Gojkovic, T.R. Vidakovic, D.R. Durovic, J. Electrochim. Acta 48 (24) (2003) 3607–3614.
[23] L. Liu, C. Pu, R. Viswanathan, Q. Fan, R. Liu, E.S. Smotkin, in: E.J. Cains (Ed.), Carbon Supported and Unsupported Pt–Ru Anodes for Liquid Feed Direct Methanol Fuel Cells, Fuel Cells, vol. 43 (24), Pergamon Press, 1998, pp. 3657–3663.
[24] A. Kabbabi, R. Faure, R. Durand, B. Beden, F. Hahn, J.M. Leger, C. Lamy, J. Electroanal. Chem. 444 (1) (1998) 41–53.
[25] J.P. Meyers, J. Newman, J. Electrochem. Soc. 149 (6) (2002) A718–A728.
[26] V.B. Oliveria, D.S. Falcão, C.M. Rangel, A.M.F.R. Pinto, J. Hydrogen Energy 32 (2007) 415–424.